Central European Journal of Energetic Materials, **2013**, *10*(3), 419-438
ISSN 1733-7178

Quantitative Analysis of α-CL-20 Polymorphic Impurity in ε-CL-20 using Dispersive Raman Spectroscopy

Mrinal GHOSH [1*], V. VENKATESAN [2*], Nirmala SIKDER [1] and Arun Kanti SIKDER [1]

[1] *High Energy Materials Research Laboratory, Sutarwadi, Pune-411 021, India*
[2] *Research & Innovation Centre, IIT Madras Research Park, Chennai-600 113, India*
[*] *E-mail: mri_444@yahoo.co.in; vvigcar@yahoo.com*

Abstract: α-CL-20 polymorphic impurity in ε-CL-20 studies have been carried out using Dispersive Raman Spectroscopy. ε-, β-, α- and γ-CL-20 polymorphs were produced using crystallization methods with sample recovery from the solution being >90%, and chemical purity of about 99%. The polymorphs prepared were characterized using Dispersive Raman Spectroscopy over the Raman shift region of 100-3500 cm^{-1} using a 514 nm argon ion laser. The experimental studies were supported by *ab initio* computations performed at B3LYP level using a 6-31+G** basis set. The computed vibrational frequencies of the CL-20 conformers correspond to the ε, β and α or γ-CL-20 polymorphs when compared with the observed frequencies. α-CL-20 shows a distinct feature at 280 cm^{-1} as compared with those of the ε-CL-20 polymorph. Using Dispersive Raman Spectroscopy, a linear relationship was demonstrated for the absolute peak height and absolute peak area ratio of α-CL-20 versus the weight percent of α-CL-20. This method enables a detection limit of this polymorphic impurity down to 2 wt%.

Keywords: CL-20, polymorphs, α-CL-20 impurity, Dispersive Raman Spectroscopy

Introduction

2,4,6,8,10,12-Hexanitro-2,4,6,8,10,12-hexaazaisowurtzitane (CL-20) is one of the most promising candidates for explosive and propellant formulations,

as it exhibits higher oxygen balance, density and heat of formation than RDX and HMX, the conventional energetic nitramines. It was first prepared by Neilsen *et al*. [1] and later the explosive performance of ε-CL-20 was found to be approximately 14% higher than that of HMX [2]. The basic skeleton of the CL-20 molecule (Figure 1) is a rigid isowurtzitane cage that contains two five membered rings and a six membered ring. The presence of six nitro groups on each bridging nitrogen atom along with the cage strain in the CL-20 molecule facilitates the rapid release of high energy. Due to both the spatial orientation of the nitro groups in the CL-20 molecule relative to the five and six membered rings of the cage, and the differences of the packing arrangements in the crystal lattice, CL-20 has been reported to exist in five different polymorphic forms. Four of them, the ε, β, α, and γ are stable at ambient conditions and can be isolated by crystallization and one (ζ) exists only at high pressure [3-6]. Further, systematic studies on the pressure and temperature dependency of CL-20 phase stability, relating particularly to the ε- and γ- phases have been reported by Jared Gump [7], and to the crystallographic parameters of ζ-CL-20 by Millar *et al.* [8]. The molecular structures of the ε-, β-, α-, γ- and ζ-CL-20 polymorphs are as shown in Figure 2. The crystal habits of all of the polymorphic forms of CL-20 under ambient conditions have been reported [5, 9] on the basis of scanning electron microscopic studies. ε-CL-20 is the phase of interest because of its highest density (2.044 g/cc) as compared to the other polymorphic forms [1, 2]. Furthermore, the higher density materials show a higher rate of detonation and maintain greater stability towards shock. Hence, the characterization of different crystal phases and the quality of energetic materials are the most important factors in view of the performance and sensitivity behavior of a particular material [10-12]. It is well-known that the material purity, particularly the polymorphic purity and crystal quality (in terms of single crystal or polycrystalline habit; sharp or rounded crystal edges; presence and absence of defects in the crystal) can greatly influence the sensitivity of energetic crystals. Other than sensitivity behavior, bulk density, mechanical strength, storage and handling can also be very different for different polymorphs. It is therefore necessary to ensure polymorphic purity, which is one of the primary measures of end-product quality.

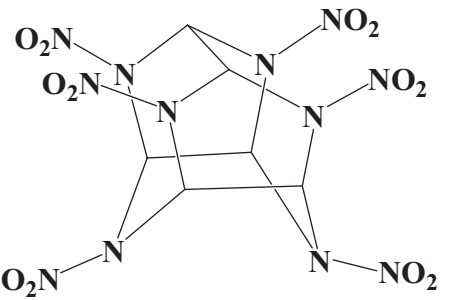

Figure 1. Basic skeleton of CL-20.

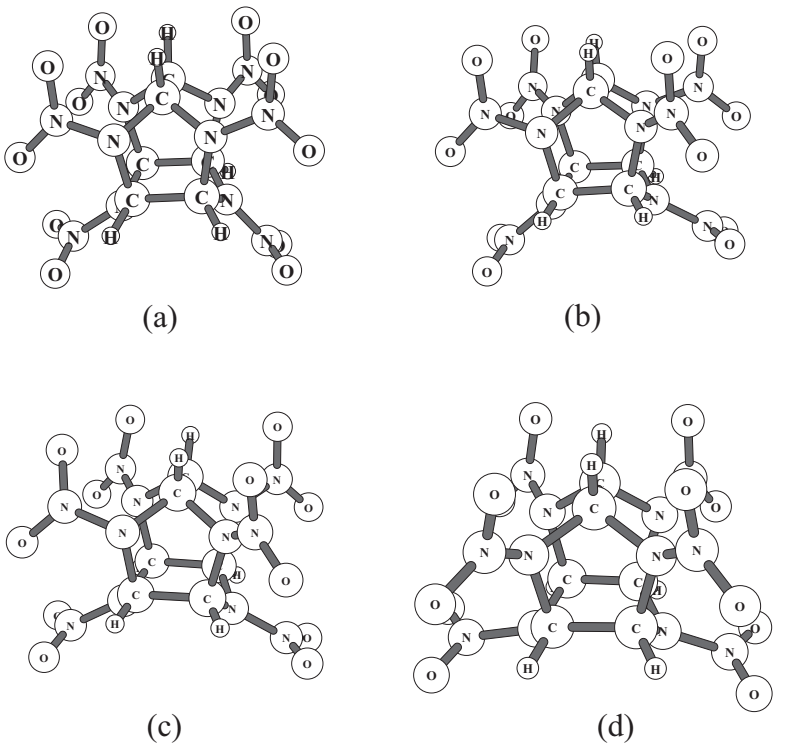

Figure 2. Molecular structures of (a) ε-, (b) β-, (c) α- or γ- and (d) ζ-CL-20 polymorphs.

The synthetic methodology as adopted worldwide for large scale production of CL-20 always yields the low density α-CL-20 as the final product. Agencies producing this material thus have also developed large scale crystallization methodologies [13, 14] for conversion of this low density α-CL-20 to the

desired high density ε-CL-20 phase. However, the crystallization process is highly sensitive to moisture and thus susceptible to producing measurable amounts of the hydrated, low density α-CL-20 phase along with ε-CL-20. Hence, the quantification of α-CL-20 impurity in ε-CL-20 is of high importance in the industrial production scale. To determine this polymorphic impurity, analytical techniques, mainly, spectroscopic techniques are an attractive choice. In particular, the use of vibrational spectroscopy, such as Fourier transform infrared (FTIR) and Raman spectroscopic techniques have been shown to be of considerable help in the characterization and identification of explosive materials based on their molecular properties and spectroscopic signatures. The vibrational pattern obtained *via* both FTIR and Raman spectroscopy for the CL-20 polymorphs are reported in the literature [15-20]. Using FTIR spectroscopy, NATO reported the upper detection limit of polymeric purity as up to 95% of ε-CL-20 [21]. This is due to substantial overlapping between the intense IR spectral peaks of the different polymorphic forms of CL-20 [22, 23]. Later, Gorb *et al*. [24] developed quantification of β- and γ-CL-20 phases down to 10% and 2% (w/w), respectively, in the ε-CL-20 phase, using FT-Raman spectroscopy. However, to the best of our knowledge, there is no literature report available for the quantification of α-CL-20 present in the bulk of the ε-CL-20 phase using Dispersive Raman spectroscopy.

In this work, all four polymorphic forms, namely α-, β-, γ- and ε-CL-20 were obtained by re-crystallization in the laboratory and were examined by Dispersive Raman spectroscopy. We have also performed *ab initio* computations on the vibrational frequencies for the various conformers of CL-20, at the B3LYP/6-31+G** level, to corroborate our experimental vibrational frequencies. With reference to the spectral characteristics of production grade CL-20, obtained from an external production agency, a study has been made to quantify α-CL-20 polymorph as an impurity in the bulk ε-CL-20 phase. This is of great importance for quality control at the synthetic level as well as in formulation work where one has to ensure that no phase transformations occur during processing or storing.

Experimental

Raw CL-20 was obtained from Premier Explosive's Laboratory, India. It was obtained as a slurry in water, which is the usual practice for storage and transportation of explosive materials as per safety guidelines. The wet sample was first air dried at room temperature and then in a water-jacketed oven at about 60 °C for several hours. The moisture content of dried CL-20 was found

to be ~0.75-1.5% (w/w), as determined using the Karl Fisher method. The desired polymorphs were then obtained by re-crystallization of raw CL-20. The α-CL-20 was obtained from acetone and the β-CL-20 by solvent evaporation of a CL-20 solution in the presence of a suitable hydrocarbon non-solvent. ε-CL-20 was prepared through the solvent:non-solvent precipitation method following literatures reports [19, 20]. The γ-CL-20 was isolated as the solidified material in an intermediate step during the preparation of ε-CL-20, rather than *via* heating the α-CL-20 to a higher temperature as reported by Foltz *et al*. [5], which is possibly hazardous from a safety point of view. All of the solvents and associated chemicals used for the processes were of analytical grade with >99% purity. The prepared polymorphs were dried in the oven at around 50 ºC for about an hour. The dried CL-20 polymorphs were well characterized using high performance liquid chromatography, vibrational spectroscopic and microscopic techniques. Morphological information of the raw CL-20 sample was obtained with a Quanta 200 Scanning Electron Microscope (SEM) from FEI, The Netherlands, so as to ascertain the exact agglomerated state at high magnification. The morphological information of the pure polymorphs as subsequently generated was obtained by a Leica DM2500 research grade optical microscope. The instrument used for the vibrational spectroscopic study was a Renishaw 'in Via Reflex' micro Raman, a dispersive Raman spectrophotometer hyphenated with an optical microscope. The motorized XYZ stage of the microscope had a translation step size of 1 μm along all three axes. The spectrometer was equipped with a 300 mW, 785 nm diode laser and a 50 mW, 514 nm air-cooled argon ion laser with the option to select sixteen levels of laser power from 0.0001% to 100%. The spectrometer uses an air-cooled CCD detector for scattered light acquisition. The vibrational Raman spectra of CL-20 obtained with both of the lasers were compared, and no significant changes in the Raman shift values were noted except for a change in peak intensity for certain features. Considering the fact of obtaining higher peak intensities with low wave length laser light *i.e*. higher Raman cross section, all the Raman spectra were collected over 100-3500 cm^{-1} relative to the laser line used, 514 nm. A comparatively low laser input power (~10%) was employed to prevent possible sample damage with two scans being co-added and at 1 cm^{-1} resolution. Multiple acquisitions were practised while examining both the pure polymorphs and also the standard mixtures, to yield sufficient collection intensity with minimized background. Each polymorph was weighed accurately and the mixtures were ground for about 10 min to ensure a high homogeneity of mixing. To prepare a sample pellet for Raman spectroscopic measurement, about 60 mg of sample mixture was pressed at a constant pressure (15 ton) and for about 5 min using pellet press equipment.

Computational

Density functional molecular orbital calculations were performed using the Gaussian 94W program [25]. Structure optimizations were done at B3LYP level with analytical gradients, using a 6-31+G** basis set, to obtain minima corresponding to the various CL-20 conformers, which correspond to ε, β, α and γ-CL-20 polymorphs. All geometric parameters were allowed to be optimized, and no constraints were imposed on the molecular geometry during the optimization process. The vibrational frequencies were calculated at the B3LYP/6-31+G** level. All computed frequencies were scaled with a uniform scaling factor of 0.9806 [26]. Raman intensities were determined by the RAINT program [27] using values of the Raman scattering activities obtained from the Gaussian outputs. Subsequently, a suitable common normalization factor was chosen for all peak intensities. The B3LYP computed frequencies and the relative intensities of the various modes for the conformers of CL-20 were then used to simulate the vibrational spectra. The spectra were constructed assuming a Lorentzian line profile with a full-width, half maximum (FWHM) of 2 cm^{-1}.

Results and Discussion

Characterization of CL-20 polymorphs

The raw CL-20 sample was used to generate the ε, β, α and γ-CL-20 polymorphs. Sample recovery from the solution was >90% with a chemical purity of about 99%, as analyzed by HPLC. Figure 3 shows the scanning electron microscope (SEM) picture of the raw CL-20. It shows a high degree of agglomeration with a mean particle size of about 185 μm. The agglomerates consist of irregular crystal geometry, dominated by sharp-edged, diamond-shaped crystals. Figure 4 shows the optical microscopic images of all of the four polymorphs generated in our laboratory. ε-CL-20 was prepared by the solvent-antisolvent crystallization method from the raw CL-20. The ε-CL-20 crystals obtained are free of agglomeration with well defined morphology and mean particle size of about 120 μm, in contrast to those of raw CL-20 (Figure 4a). The crystal morphology of ε-CL-20 prepared by the precipitation method shows predominantly bi-pyramidal shape. Similarly, α-CL-20 was obtained by the crystallization of raw CL-20 from a saturated solution in acetone. The α-CL-20 obtained shows diamond shaped crystals with an approximate particle size of 150 μm (Figure 4b). The morphology of the ε-CL-20 and α-CL-20 polymorphs obtained compare well with the reported morphology [5, 9]. In contrast to the shape of the ε-CL-20 and α-CL-20 crystals,

β-CL-20 forms long needle-shaped crystals. These assume rectangular rod shapes with very sharp, conical ends, indicating the preference for axial growth during crystallization. The particles vary in length from 30 to 75 μm, with smaller diameters of around 15 μm on average. Because of their needle shape, these particles exhibit a very high aspect ratio (L/D), which mainly contributes to their higher sensitivity towards friction and impact. By contrast, the γ-CL-20 prepared does not show any regular morphology, as shown in Figure 4d. All of the crystals of the CL-20 polymorphs exhibit typical habits, except γ-CL-20, so that they can be distinguished without any difficulty.

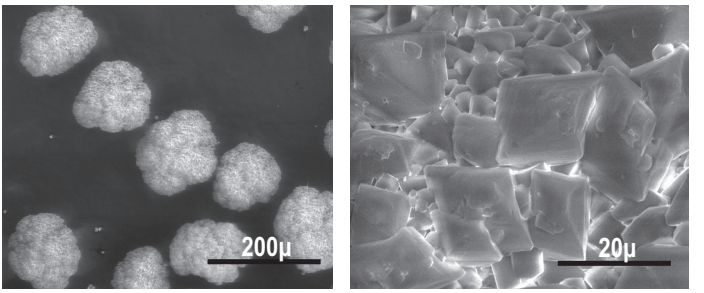

Figure 3. SEM images of raw CL-20 showing a high degree of agglomeration.

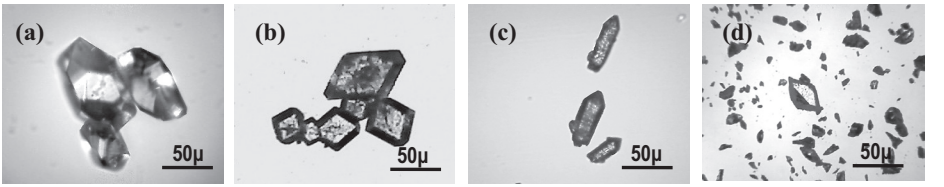

Figure 4. Optical microscopic images of (a) ε-, (b) α-, (c) β- and (d) γ- CL-20 polymorphs.

Figure 5 shows the Raman spectra of the CL-20 polymorphs over the region 100-3500 cm^{-1}. The regions of 3000-3075, 1200-1650, 700-900 and 240-360 cm^{-1} correspond mostly to CH stretching; CH bending and NO_2 stretching; bending (NO, NNO and ONO); CNN bending and cage deformation vibrations, respectively, are presented in Figures 6a-d. Tables 1 and 2 show the experimental frequencies of the CL-20 polymorphs, along with the previously reported literature values, respectively [28-29]. Of interest to this work are the peaks which are unique to the different polymorphs. This makes it necessary to look at the spectra in more detail. Since, we are particularly interested in detecting the α-CL-20 polymorphic impurity in ε-CL-20, we carefully compared the spectra of ε- and α-CL-20 to find regions where intense α-CL-20 peaks had minimal overlap with the ε-CL-20 peaks. The

first region of 3000-3075 cm^{-1} (Figure 6a), dominated by the C-H stretching bands observed in all of the polymorphs, shows significant overlapping and hence it is very difficult to use these features for the exclusive identification of particular polymorphs. The main C-H stretching spectral features of the ε-CL-20, α-CL-20, β-CL-20 and γ-CL-20 polymorphs occur at 3048, 3056, 3045 and 3043 cm^{-1}, respectively. The region shown in Figure 6b, extending from 1200 to 1650 cm^{-1}, critically shows the symmetric and asymmetric NO_2 stretching and CH bending vibrations. This region shows multiple peaks substantially overlapping each other for all of the phases. The symmetric and asymmetric NO_2 stretching vibrations of the ε-CL-20 polymorph occur at around 1310 and 1625 cm^{-1} respectively. The CH bending vibrations as reported by Leszczynski *et. al*. [29], for the ε-CL-20 phase are in the range 1325 to 1350 cm^{-1}.

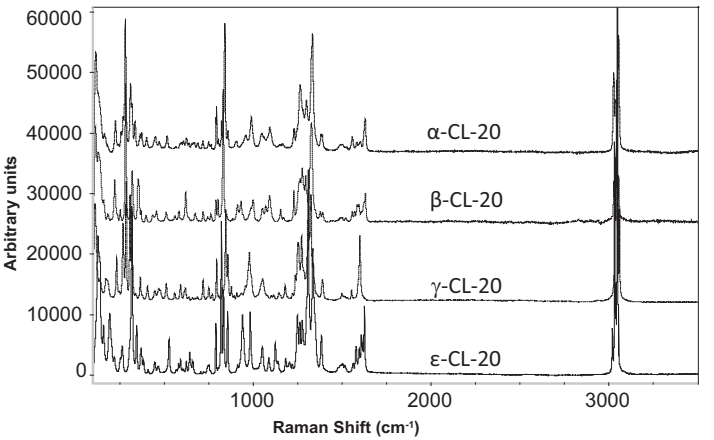

Figure 5. Raman spectra of α-, β-, γ- and ε-CL-20 polymorphs in the range 100-3500 cm^{-1}.

The experimental values obtained for ε-CL-20 exhibit two well separated, strong vibrational bands at 1310 and 1336 cm^{-1}. By contrast, the γ-CL-20 phase shows closer bands at 1310 and 1324 cm^{-1}. The α- and β-CL-20 phases however, show broad single bands at 1333and 1328 cm^{-1}, respectively. The region 700 to 900 cm^{-1} is populated by individual peaks of moderate intensity as well as by strong peaks overlapping each other (Figure 6c). Some peaks characteristic for each polymorph are found at around 800 cm^{-1}. Strong bands at 839, 832, 846 and 819 cm^{-1} are characteristic for the α-, β-, γ- and ε-CL-20 polymorphs, respectively. In the 240-360 cm^{-1} region, the main spectral features with appreciable intensity for the ε-CL-20 polymorph occur at 264 and 344 cm^{-1} (Figure 6d). ε-CL-20 shows a single Raman feature at 264 cm^{-1} in the region of 240-360 cm^{-1}, corresponding to cage deformation, whereas this is at 280, 282 and 286 cm^{-1} respectively for α-CL-20,

β-CL-20 and γ-CL-20. The distinct feature close to 280 cm^{-1} is clearly absent in ε-CL-20, whereas it is found in all of the other CL-20 polymorphs. In contrast to α-CL-20, ε-CL-20 shows a distinct feature with moderate intensity at 344 cm^{-1}.

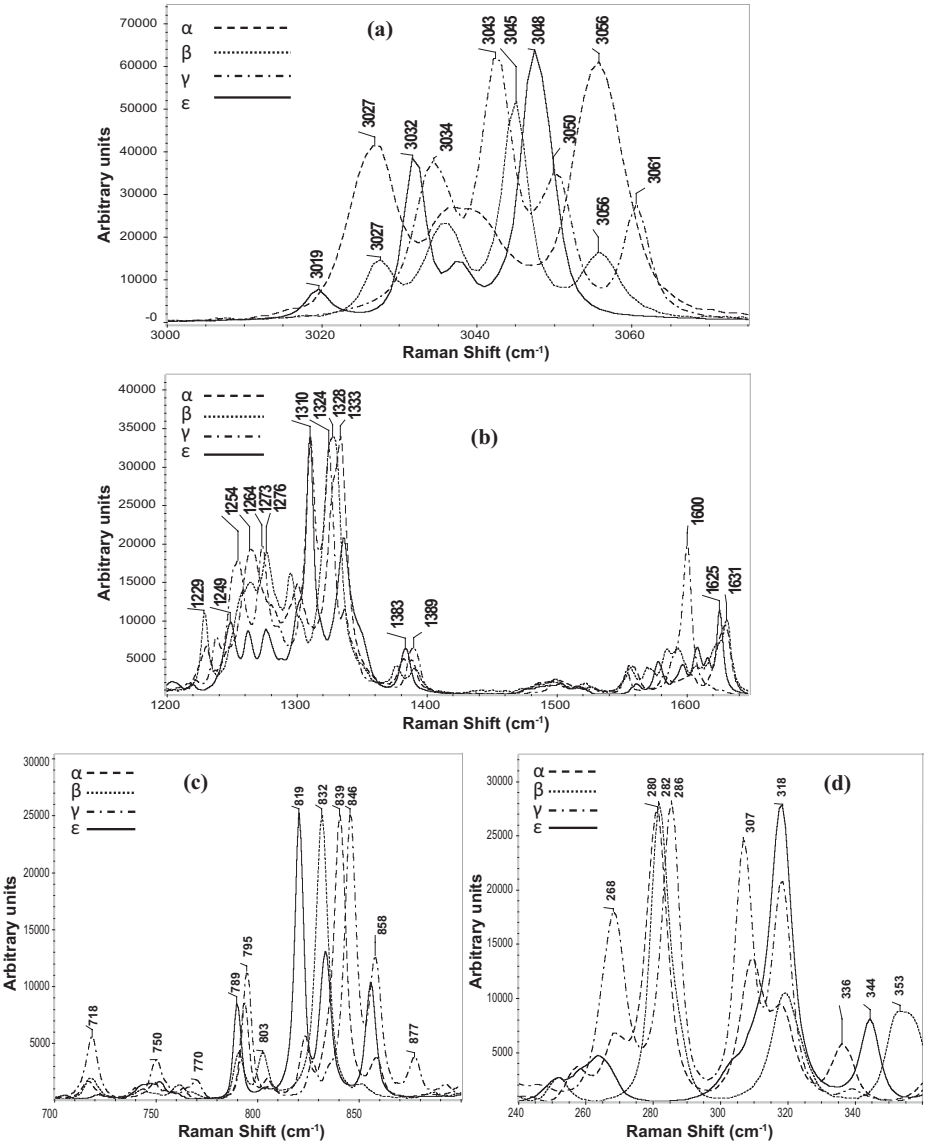

Figure 6. Raman spectra of α-, β-, γ- and ε-CL-20 in: (a) 3000-3075 cm^{-1} region; (b) 1200-1650 cm^{-1} region; (c) 700-900 cm^{-1} region and (d) 240-360 cm^{-1} region.

Table 1. The experimental and computed[a] Raman frequencies of ε- and β- CL-20 polymorphs along with literature data [29]

ε-CL-20 [cm^{-1}]			β-CL-20 [cm^{-1}]			**Tentative Assignments**
Experiment	Literature	Computed	Experiment	Literature	Computed	
127,136 s		103(2),[b] 106(21), 117(2), 139(0)	114, 129 m		101(3), 102(10), 116(2)	N-N tors, CNN bend
158 w		155(2)	160 w		149(1), 153(0)	CCN bend
193 m		201(8)	182 vw			cage def
219 w		232(6)	222 w		203(14)	SMR def
					213(0)	cage def
			252 vw		247(2)	cage def
264 w	267w	244(4), 249(11)				cage def
			282 s	284s	265(31), 267(7)	cage def
318 s		289(7), 299(9), 304(72)	319 m		307(28), 313(5)	cage def, CNN bend
344 m		324(22)				cage def
369,383w		351(12), 361(3), 373(5)	353, 369 w		333(14), 345(10), 360(3)	cage def , N-NO_2 bend
			398 vw		387(5)	N-NO_2 bend
409 vw		394(1)				N-NO_2 bend
446 vw		436(3)	435,456 vw		423(3), 443(2), 455(3)	N-NO_2 bend
465 vw		450(8)				NNO bend
527 w		516(14)	511 vw		500(4)	NNO bend
					544(6)	NNO bend
568, vw		562(2), 568(8)	560 vw		568(4)	cage def
580, 591,605 vw		580(4), 595(2)	583 vw		587(0), 605(4)	cage def
624 vw		617(3), 634(6)	621 w		616(5), 637(1)	cage def
643 w		643(0)			646(0)	cage def
660 vw		654(8)				cage def
		692(0)	673 vw		666(3), 667(1)	NO bend
721 vw		718(2), 721(1), 731(1), 735(0), 738(2)	718 vw		712(4), 722(1)	NO bend; NNO_2 bend
					731(1)	
752 vw	755 w	740(1), 747(0), 749(0)	744 vw		738(3), 739(1)	ONO bend
			762 vw	763w	750(0), 751(0), 757(1)	ONO bend
790w	791w	781(20), 791(0)	791, 803 w	792,805w	784(19), 792(3)	ONO bend
819 s	820s	807(25), 816(3)			811(0), 820(1)	ONO bend
832 m	832w	824(30)	832 s	835m	823(33), 841(9)	ring CH wag

855m	857w	843(10), 868(0)	852 vw	854w	871(1)	ring CH wag
912, 940 m		897(6), 903(3), 917(3), 929(14), 939(3), 945(0) 963(14)	912, 932, 944 w		896(1), 902(8), 917(1), 926(16), 937(1)	ring str; ring CH wag
983 m		1002(20)	982, 999 w		958(6), 965(3), 966(15)	NN str
		1023(5)				NN str
1051 w	1055vs	1041(58)	1052, 1071vw	1055, 1076s	1041(29), 1075(2)	NN str
1088 w	1080w	1074(3)	1093 w	1090vs	1085(3), 1088(40)	NN str
					1126(2)	NN str
1124m, 1139 w	1115w, 1125s	1117(33), 1120(5), 1128(11)		1125w		CH bend
			1154 vw	1155m	1155(9), 1157(2)	CH bend
1183 vw	1180w	1176(4)		1175m	1179(2)	CH bend
	1190m			1188m	1187(0)	CH bend
1204, 1219vw		1190(5), 1198(5), 1222(4)				CH bend, NCN bend, CNN bend
1249m 1262,1276w		1238(8), 1251(4), 1260(27), 1263(20) 1276(6), 1277(26), 1285(20), 1287(5)	1229 w, 1264,1276 m		1233(10), 1235(1), 1256(2), 1264(24), 1270(14), 1278(17), 1278(17)	CH bend ; NO str sym
1310 vs		1298(17), 1304(23), 1314(11), 1325(19), 1346(78)	1295 w		1285(5), 1288(24)	CH bend ; NO str sym
1336 s		1352(0), 1353(34)	1328 s		1304(0), 1308(22), 1320(3), 1320(13), 1339(1), 1346(90), 1353(1), 1357(2)	CH bend
1383 w		1388(16), 1389(1)	1377,1390vw		1391(11), 1394(2),	CH bend
1503 vw			1496 vw			
1561 vw, 1578 w 1597,1608, 1616w, 1625m		1616(4), 1622(5), 1640(7), 1649(10), 1652(12), 1663(27)	1557 vw, 1570 vw, 1585,1593 w, 1631 w		1618(4), 1619(4), 1646(4), 1646(6), 1660(18), 1661(12)	NO str asym
3019 m, 3032 s, 3038 m, 3048 vs	3020w, 3031m, 3048vs	3116(5), 3121(51), 3125(11), 3130(100) 3134(79), 3144(70)	3027 w, 3036 m, 3045 s 3056 m	3035m, 3045m, 3055m	3121(11), 3122(3), 3127(16), 3128(100), 3142(7), 3148(74)	CH str

Notes: vs – very strong; s – strong; m − medium; w – weak; vw – very weak; SMR – six-membered ring of CL-20. [a]The calculation level is B3LYP/6-31+G**. A scaling factor 0.9806 is applied. [b]Values in parentheses are computed relative Raman intensities.

Table 2. The experimental and computed[a] Raman frequencies of α- and γ- CL-20 polymorphs along with literature data [29]

α-CL-20 [cm^{-1}]		γ-CL-20 [cm^{-1}]		Computed	Tentative Assignments
Experiment	Literature	Experiment	Literature		
115, 130 m		110 m, 140 w		103(9),[b] 116(2)	N-N tors, CNN bend
164 w		172 w		149(1), 155(1)	CCN bend
226 w		232 w		215(9)	cage def
257 w				237(2), 245(9),	cage def
268 w		268 m	270w	256(7)	cage def
280 s	283s	286 s	287w	269(25)	cage def
310, 318 m		307, 318 m		298(43), 304(5)	cage def
336 w		340 vw		322(6)	cage def
365, 374 w		366 w		356(5), 361(3)	cage def
401 w		406 w		393(2)	N-NO_2 bend
		447 vw		429(1)	N-NO_2 bend
450, 471w		470,479 vw		446(8), 474(4)	N-NO_2 bend
515 w		512 w		521(9),	N-NO_2 bend
564,w		560 vw		550(5), 573(4)	N-NO_2 bend
590, 597, 608vw		592 w, 613,619 w		584(2), 597(4), 608(4)	cage def
625 w, 640 vw		639 vw		633(2),	cage def
656,666 vw				659(3), 662(3)	cage def
689 vw		686 vw		679(3)	ONO bend
717 vw		718 w		712(4), 725(1)	ONO bend
				732(0)	ONO bend
749, 763vw	762w	750 vw, 770 vw	762w	736(1), 742(0), 746(0), 752(0), 754(0)	ONO bend
793, 805m	795w	795 807 w	795w	785(19), 794(1)	ONO bend

822 w	825w	827 vw	836w	814(5), 820(4)	ONO bend
839 s	842m	846 m	849m	832(25), 846(13)	ring CH wag
858 w	861w	858 m	861w	867(1)	ring CH wag
		877 w		887(3)	ring CH wag
906 vw		909		903(2), 921(1)	ring CH wag
958 w		935 vw		937(6), 947(12), 952(5)	ring str; ring CH wag
989 w		956, 978 w		961(10), 973(4)	ring str; ring CH wag
				1013(12)	ring str; ring CH wag
1048 w	1054s	1055 w	1060s	1036(45)	ring str; NN str
1093 w	1095vs		1083m	1071(3), 1089(26)	ring str; NN str
	1120sh		1105m	1112(2), 1127(8)	NN str
1148vw	1150m	1145 vw	1148m	1152(4)	CH bend ; ring str
1168 vw	1170m	1179 w	1180w	1171(2), 1184(2)	CH bend ; ring str
	1192w				CH bend
1230 w		1220vw, 1238 w		1230(3), 1237(6)	CH bend
1264,1282m		1254, 1273m		1253(5), 1263(29), 1266(19), 1271(8), 1281(8), 1284(9), 1286(24), 1293(5)	CH bend ; NO str sym
1300 m		1310		1301(16), 1316(6), 1324(3), 1340(3)	CH bend ; NO str sym
1333 s		1324 s , 1336 w		1345(100), 1353(6), 1359(1)	CH bend ; NO str sym
1382,1389w		1389 w		1384(5), 1394(5)	CH bend
1500 vw, 1557 w, 1583, 1603w, 1630 w		1498 vw, 1554 vw, 1600 m		1617(3), 1633(3), 1641(3), 1647(10), 1657(13), 1660(20)	NO str asym
3027 m, 3037 m, 3056 s	2924w , 3028m, 3038m, 3058s	3034 s, 3043 s, 3050 s, 3061 m	3035w, 3044m, 3062m	3118(13), 3126(20), 3128(23), 3133(67), 3138(5), 3146(74)	CH str

Notes: vs – very strong; s – strong; m – medium; w – weak; vw – very weak; [a]The calculation level is B3LYP/6-31+G**. A scaling factor 0.9806 is applied. [b]Values in parentheses are computed relative Raman intensities.

The vibrational frequencies were calculated at the B3LYP/6-31+G** level for three conformers, corresponds to the ε, β and α or γ-CL-20 polymorphs, using analytical gradients. The scaled computed frequencies are listed in Tables 1 and 2, together with the experimental values. In Figures 7 and 8, we compare the experimental spectra with the computed synthetic spectra obtained by the scaled computed vibrational frequencies for the CL-20 conformers, corresponding to the ε, β and α or γ-CL-20 polymorphs. It can be seen that there is agreement between the experimental and computed spectra. As can be seen from Tables 1 and 2 and Figures 7 and 8, Raman activity in the region of 250-300 cm^{-1} is low for the CL-20 conformer corresponding to the ε polymorph as compared to the other polymorphs. This observation is in agreement with the experimental vibrational frequencies. The increased intensity in the computed features at 269 and 265 cm^{-1} in the α- or γ-CL-20 and the β-CL-20 conformers is therefore assigned to those of the corresponding experimental feature at 280 or 286 and 282 cm^{-1}, respectively. In the 750-880 cm^{-1} region, the conformer corresponding to the ε-CL-20 polymorph shows a multiplet feature with increased intensity at around 800 cm^{-1} and is in agreement with those of the experimental observations (Figures 7a and 7b). The computed spectra of the conformers studied have not shown significant differences in the regions of C-H stretching (3100-3150 cm^{-1}) and bending (1200-1400 cm^{-1}), as observed in the case of the experimental spectra.

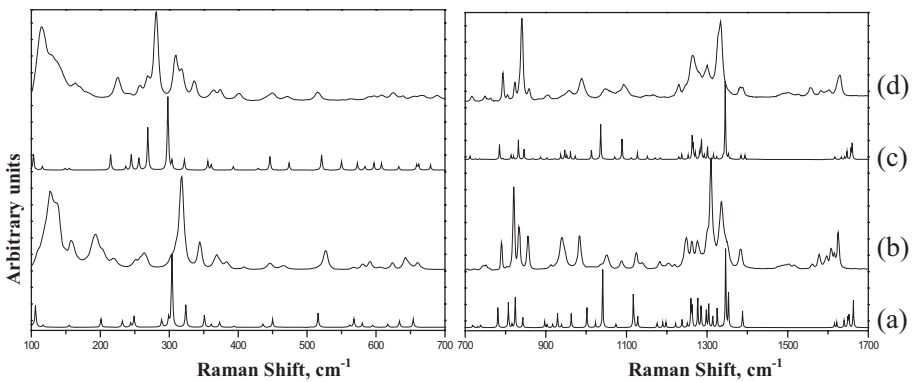

Figure 7. Comparison of computed and experimental Raman spectra for CL-20 in the region 100-700 cm^{-1} and 700-1700 cm^{-1}: Computed spectra for the molecular conformers corresponds to (a) ε- and (c) α or γ-Cl-20 polymorphs. Experimental Raman spectra of (b) ε- and (d) α-Cl-20 polymorphs.

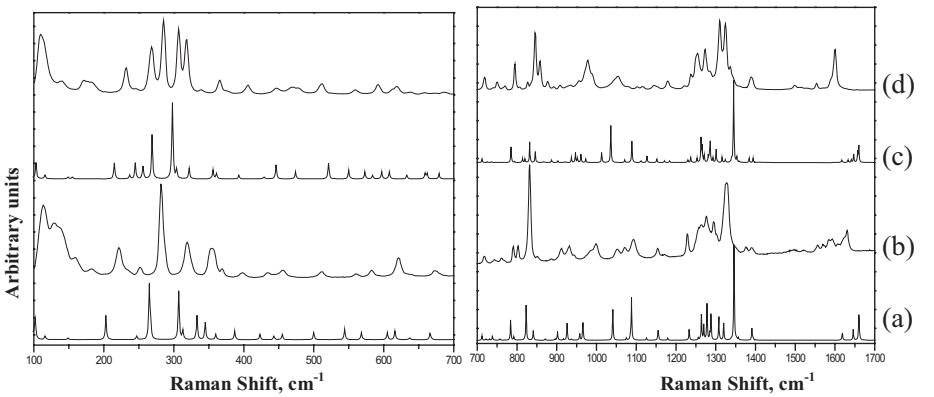

Figure 8. Comparison of the synthetic and experimental Raman spectra for CL-20 in the region 100-700 cm^{-1} and 700-1700 cm^{-1}: Computed spectra for the molecular conformers corresponds to (a) β- and (c) α or γ-Cl-20 polymorphs. Experimental Raman spectra of (b) β- and (d) γ-Cl-20 polymorphs.

Quantitative analysis of α-CL-20 polymorphic impurity in ε-CL-20

As discussed earlier, in the complete spectrum (100-3500 cm^{-1}), a distinct feature exists at 280 cm^{-1} which is characteristic for the α-CL-20 polymorph, and by detailed examination it is evident that it is possible to determine this polymorphic impurity in an unknown sample of ε-CL-20. Furthermore, the ε-CL-20 peak at 344 cm^{-1} was selected for measuring the ε-CL-20 concentration because it had minimal overlap with the peaks of the α-form. The peak area and peak height were employed as parameters to quantify the level of the polymorphic impurity. Using a dispersive Raman spectrometer, a linear relationship was demonstrated for the absolute peak area of α-CL-20 versus the weight percent of α-CL-20. Mixtures containing α-CL-20 in the proportions of 1-8 wt% were prepared by weighing out the proper amounts of each polymorph (α- and ε-CL-20). The Raman shifts of these mixtures were then recorded. Figure 9 shows the Raman spectra for mixtures of the polymorphs with different weight percentages of α-CL-20 = 2.082, 4.072, 6.063 and 7.996 wt% covering the spectral region 240-360 cm^{-1}. The most pronounced feature is the increasing intensity of the α-CL-20 peak at 280 cm^{-1}. The mixture containing 0.998 wt% (~1%) of the α-phase however, does not show detectable Raman scattering intensity at 280 cm^{-1} above the baseline. Sample preparation for quantitative analysis is very critical, as one has to maintain a particle size comparable to the laser spot size (~0.8 μm at the focal point for a 20x objective) and homogeneity of mixing as far as physical mixing of two solids is concerned. In order to reduce the in-homogeneity of the sample mixture, we repeatedly pressed the powder under

a pressure of up to 15 tons using a pellet die and then re-crushed each disc. A pressed disc was finally used for analysis. A line scan through a 100 μm length over the surface of the pressed pellet of the standard mixtures, with a step size of 5 μm, was preferred, and thus a total of twenty one spectras were collected per mixture. Averaging of these twenty one spectra yielded an almost true representative spectrum for the inhomogeneous solid mixtures. Both the peak height and the peak area were employed as parameters to quantify the polymorphic impurity level. The ratio of the peak areas and peak heights at 280 and 344 cm^{-1} for each mixture were plotted against the corresponding wt% α-CL-20 polymorph as shown in Figures 10 and 11, respectively. A good linearity was observed in both the plots. The study thus could establish the lower detection limit of the α-CL-20 phase present in ε-CL-20 is about 2 wt% using Dispersive Raman Spectroscopy.

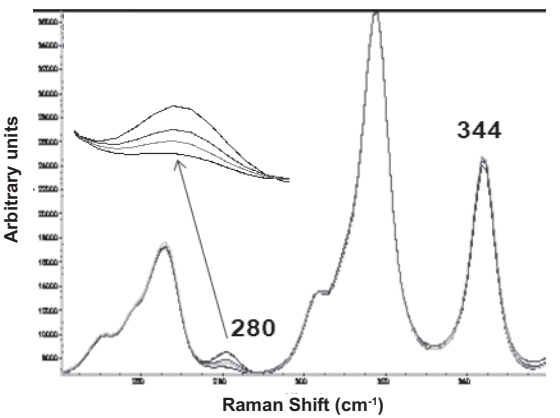

Figure 9. Overlay profile of the averaged spectra in 240-360 cm^{-1} of 2-8 wt% of α-CL-20 in the mixtures.

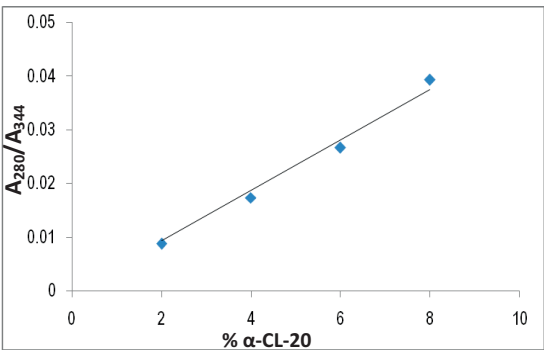

Figure 10. Plot of peak area ratios against the corresponding wt% α-CL-20 in the mixtures.

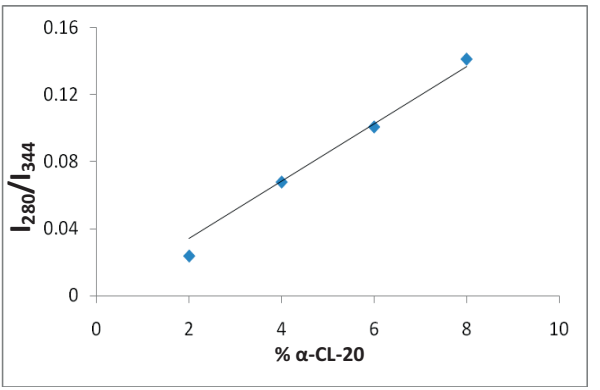

Figure 11. Plot of peak height ratios against the corresponding wt% α-CL-20 in the mixtures.

Conclusions

ε-, β-, α- and γ-CL-20 polymorphs were produced using crystallization methods, with the sample recovery from the solution being >90% and chemical purity of about 99%. The computed vibrational frequencies of the CL-20 conformers corresponded to the ε, β and α or γ-CL-20 polymorphs by comparison with the observed frequencies. α-CL-20 shows a distinct feature at 280 cm^{-1} as compared with those of ε-CL-20 polymorph. This observation was in agreement with those of the computational results. Furthermore, the ε-CL-20 peak at 344 cm^{-1} was selected as a distinct feature of the ε-CL-20 polymorph because it had a minimal overlap with the peaks of the α-CL-20 form. Using Dispersive Raman Spectroscopy, a linear relationship was demonstrated for the absolute peak height and absolute peak area ratio of α-CL-20 versus the weight percent of α-CL-20. This method enables detection of the α-CL-20 polymorphic impurity down to 2 wt%.

Acknowledgements

The authors are highly obliged to Shri B Bhattacharya, Outstanding Scientist and Director, HEMRL, for his support in carrying out this work.

References

[1] Nielsen A.T., Polycyclic Amine Chemistry, in: *Chemistry of Energetic Materials*, (Olah G.A., Squire D.R., Eds.), Academic Press, San Diego, US, **1991**, pp. 95-124.

[2] Simpson R.L., Urtiew P.A., Ornellas D.L., Moody G.L., Scribner K.J., Hoffman D.M., CL-20 Performance Exceeds that of HMX and Its Sensitivity is Moderate, *Propellants Explos. Pyrotech.*, **1997,** 22, 249-255.

[3] Yee R.Y., Nadler M.P., Neilsen A.T., Polymorphic and Thermal Properties of Hexanitrohexaazaisowurtzitane, *1990 JANNAF Prop. Meeting, Anaheim CA*, **1990**, 204.

[4] Russel T.P., Miller P.J., Piermarini G.J., Block S., High Pressure Phase Transition in γ- Hexanitrohexaazaisowurtzitane, *J. Phys. Chem*., **1992**, *96*, 5506.

[5] Foltz M.F., Coon C.L., Garcia F., Nicholas III A.L., Thermal Stability of the Polymorphs of Hexanitrohexaazaisowurtzitane. Part I, *Propellants Explos. Pyrotech.*, **1994**, *19*, 19-25.

[6] Nielsen A.T., Chafin A.P., Christian S.L., Moore D.W., Nadler M.P., Nissan R.A., Vanderah D.J., Synthesis of Polyazapolycyclic Caged Polynitramines, *Tetrahedron*, **1998**, *54*, 11793-11812.

[7] Gump J., Phase Stability of Epsilon and Gamma HNIW (CL-20) at High-Pressure and Temperature, *American Physical Society, 15th APS Topical Conference on Shock Compression of Condensed Matter*, **2007**, abstract #H7.004.

[8] Millar D.I.A., Maynard-Casely H. E., K.K. Annette, Marshall W.G., Pulham C.R., Cumming A.S., Putting the Squeeze on Energetic Materials – Structural Characterization of a High-pressure Phase of CL-20, *Cryst. Eng. Comm.*, **2010**, 12, 2524-2527.

[9] Hoffman D.M., Void Density Distribution in 2,4,6,8,10,12-Hexanitro-2,4,6,8,10,12-hexaazaisowurtzitane (CL-20) Prepared under Various Conditions, *Propellants Explos. Pyrotech.*, **2003**, *28*, 194-200.

[10] Perseen P.-A., Holmberg R., Lee J., *Rock Blasting and Explsovies Engineering*, CRC press, Baca Raton, FL, **1993**.

[11] Koehler J., Meyer R., *Explosives*, 4th ed., VCH, Weinheim, **1993**.

[12] Coffey C.S., DeVost V.F., Impact Testing of Explosives and Propellants, *Propellants, Explos. Pyrotech.*, **1995**, *20*, 105.

[13] Hamilton R.S., Mancini V., Nelson C., Dressen S.Y., *High Temperature Crystallization of 2,4,6,8,10,12-Hexanitro-2,4,6,8,10,12-hexaazatetracyclo [5.5.0. $0^{5,9}$.$0^{3,11}$]—dodecane*, US Patent 7288648, **2007**.

[14] Hamilton R.S., *Crystallization of 2,4,6,8,10,12-Hexanitro-2,4,6,8,10,12-hexaazatetracyclo [5.5.0. $0^{5,9}$.$0^{3,11}$]—dodecane*, US Patent 6992158, **2006.**

[15] Holtz E.V., Ornellas D., Folts M.F., Clarkson J.E., The Solubility of ε-CL-20 in Selected Materials*, Propellants Explos. Pyrotech.*, **1994**, *19*, 206-212.

[16] Wardle R.B., Johnston G., Hinshaw J.C., Braithwaite P., Synthesis of the Cased Nitramine HNIW (CL-20), *27th Int. Annu. Conf. of ICT*, Karlsruhe, Germany, 1**996**, 27.

[17] Venkatesan V., Ghosh M., Polke B.G., Sikder A.K., Crystallization and Characterization of 2,4,6,8,10,12-Hexanitro-2,4,6,8,10,12-hexaazaisowurtzitane (CL-20) Polymorphs Coupled with ab initio Computational Studies, *7th High Energy Materials Conference and Exhibit*, Pune, India, December, **2009**.
[18] McNesby K.L., Wolfe J.E., Morris J.B., Pesce-Rodriguez R.A., Fourier Transform Raman Spectroscopy of Some Energetic Materials and Propellant Formulations, *J. Raman Spectrosc.*, **1994**, 25, 75-87.
[19] Thiboutot S., Brousseau P., Ampleman G., Pantea D., Côté S., Potential Use of CL-20 in TNT/ETPE-Based Melt Cast Formulations, *Propellants Explos. Pyrotech.*, **2008,** *33*(2), 103-108.
[20] Ostmark H., Bergman H., Sjoberg P., Sensitivity and Spectroscopic Properties of the β-and ε- Polymorphs of HNIW, *Int. Symposium on Energetic Materials Technology*, Arizona, USA, **1995**, 75-81.
[21] NATO STANAG 4566, Explosives, *Specification for e-CL-20*, NATO Military Agency for Standardization, 1110 Brussels, Belgium, September, **2004**.
[22] Bouma R.H.B., Duvalois W.A.E., Heijden Vander D.M., Steen Vander A.C., Characterization of a Commercial Grade CL-20: Morphology, Crystal Shape and Shock Initiation Testing by Flyer Impact, *31st Int. Annu. Conf. of ICT*, Karlsruhe, Germany, **2000**, 105/1-9.
[23] Torry S., Cuncliffe A., Polymorphism and Solubility of CL-20 in Plasticizers and Polymers, *31st Int. Annu. Conf. of ICT*, Karlsruhe, Germany, **2000,** 107/1.
[24] Gorb L., Leszczynski J., Goede P., Latypov N.V., Östmark H., Fourier Transform Raman Spectroscopy of the Four Crystallographic Phases of α, β, γ and ε 2,4,6,8,10,12-Hexanitro-2,4,6,8,10,12-hexaazatetracyclo[5.5.0.$0^{5,9}$.$0^{3,11}$]dodecane (HNIW, CL-20), *Propellants Explos. Pyrotech.*, **2004**, *29*(4), 205-208.
[25] Frisch M.J., Trucks G.W., Schlegel H.B., Scuseria G.E., Robb M.A., Cheeseman J.R., Montgomery Jr. J.A., Vreven T., Kudin K.N., Burant J.C., Millam J.M., Iyengar S.S., Tomasi J., Barone V., Mennucci B., Cossi M., Scalmani G., Rega N., Petersson G.A., Nakatsuji H., Hada M., Ehara M., Toyota K., Fukuda R., Hasegawa J., Ishida M., Nakajima T., Honda Y., Kitao O., Nakai H., Klene M., Li X., Knox J.E., Hratchian H.P., Cross J.B., Adamo C., Jaramillo J., Gomperts R., Stratmann R.E., Yazyev O., Austin A.J., Cammi R., Pomelli C., Ochterski J.W., Ayala P.Y., Morokuma K., Voth G.A., Salvador P., Dannenberg J.J., Zakrzewski V.G., Dapprich S., Daniels A.D., Strain M.C., Farkas O., Malick D.K., Rabuck A.D., Raghavachari K., Foresman J.B., Ortiz J.V., Cui Q., Baboul A.G., Clifford S., Cioslowski J., Stefanov B.B., Liu G., Liashenko A., Piskorz P., Komaromi I., Martin R.L., Fox D.J., Keith T., Al-Laham M.A., Peng C.Y., Nanayakkara A., Challacombe M., Gill P.M.W., Johnson B., Chen W., Wong M.W., Gonzalez C., Pople J.A., *Gaussian 03, Revision A.1*, Gaussian, Inc., Pittsburgh PA, **2003**.
[26] Scott A.P., Radom L., Harmonic Vibrational Frequencies: An Evaluation of Hartree-Fock, Møller-Plesset, Quadratic Configuration Interaction, Density Functional Theory, and Semiempirical Scale Factors, *J. Phys. Chem.*, **1996**, *100*, 16502-16513.
[27] Michalska D., Wysokiński R., The Prediction of Raman Spectra of Platinum(II)

Anticancer Drugs by Density Functional Theory, *Chem. Phys. Lett.*, **2005**, *403*, 211-217**.**

[28] Kholod Y., Okovytyy S., Kuramshina G., Qasim M., Gorb L., Furey J., Honea P., Fredrickson H., Leszczynski J., Are 1,5- and 1,7-Dihydrodiimidazo[4,5-b:40,50-e] Pyrazine the Main Products of 2,4,6,8,10,12-hexanitro-2,4,6,8,10,12-hexaazaisowurtzitane (CL-20) Alkaline Hydrolysis? A DFT Study of Vibrational Spectra, *J. Mol. Struct.*, **2006**, *794*, 288-302.

[29] Kholod Y., Okovytyy S., Kuramshina G., Qasim M., Gorb L., Leszczynski J., An Analysis of Stable Forms of CL-20: A DFT Study of Conformational Transition, Infrared and Raman Spectra, *J. Mol. Struct.*, **2007**,843, 14-25.